ACS APPLIED MATERIALS & INTERFACES

Research Article

www.acsami.org

Organic Solar Cells Based on Three-Dimensionally Percolated Polythiophene Nanowires with Enhanced Charge Transport

Joo-Hyun Kim,[†] Min Kim,[†] Hiroshi Jinnai,[‡] Tae Joo Shin,[§] Haena Kim,[†] Jong Hwan Park,[†] Sae Byeok Jo,[†] and Kilwon Cho*,[†]

[†]Department of Chemical Engineering, Pohang University of Science and Technology, Pohang 790-784, Korea

[‡]Institute for Materials Chemistry and Engineering (IMCE), Kyushu University, Fukuoka 819-0395, Japan

[§]Pohang Accelerator Laboratory, Pohang University of Science and Technology, Pohang 790-784, Korea

Supporting Information

ABSTRACT: The influence of micrometer-scale poly(3-hexylthiophene) (P3HT) nanowires (NWs) and P3HT nanocrystals (NCs) on the photocurrent generation in photoactive layers having various thickness values was investigated. Self-organizing P3HT NWs were fabricated using a marginal solvent. Transmission electron microtomography was used to characterize the vertical and horizontal crystalline morphologies of the NWs and their intergrain percolation networks in the active layers. The interpenetrating P3HT NWs promoted charge transport, as demonstrated by the enhanced percolation probability and the reduction in bimolecular recombination. The photovoltaic performances were enhanced as the photoactive layer thickness increased because internal quantum efficiencies of the solar devices prepared with active layers having NWs were maintained with varying thicknesses, suggesting that the conversion of absorbed photons into a photocurrent proceeded efficiently. By contrast, the photovoltaic performances of an NC-only photoactive layer were reduced by the increase in thickness due to its poorly developed percolation pathways. The incorporation of P3HT NWs into the P3HT:indene-C_{60} bisadduct photoactive layers yielded a device power conversion efficiency (PCE) of 5.42%, and the photocurrent did not decrease significantly up to a thickness of 600 nm, resulting in a PCE of 3.75%, 70% of the maximum PCE of 5.42%.

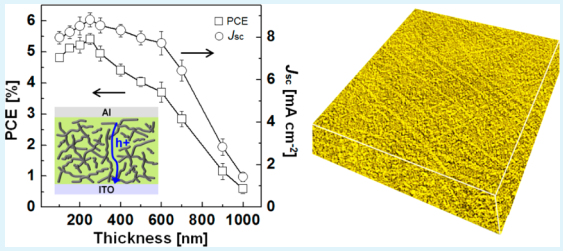

KEYWORDS: *polythiophene nanowire, photoactive layer thickness, percolation pathway, percolation probability, charge transport, transmission electron microtomography*

1. INTRODUCTION

Organic photovoltaic (OPV) devices are a promising technology for the harnessing of renewable solar energy because they are low-cost, lightweight, and flexible. Bulk heterojunction (BHJ) solar cells with nanoscale morphologies utilize a conjugated polymer as the electron donor and a fullerene derivative as the electron acceptor.[1−5] The donor and acceptor materials form an interpenetrating polymer−fullerene network developed by polymer crystallization and nanoscale phase separation. Significant efforts have been devoted to controlling the nanoscale morphologies of these organic solar cells (OSCs) in order to maximize their power conversion efficiencies (PCEs). The methods tested thus far include thermal annealing,[6−9] solvent soaking,[10−13] the use of chemical additives,[14−18] and the use of marginal solvents.[19−27] The optimal photoactive layer thickness has been determined to be 100−200 nm, although the thickness tends to be difficult to control in the context of large-area fabrication techniques and mass production.[28−32] The development of thick high-performance photoactive layers is essential for the realization of high-efficiency OPV devices.

Photocurrent generation in an OPV device is governed by the internal quantum efficiency (η_{IQE}) and the light absorption efficiency (η_A).[33,34] η_{IQE} involves the steps of exciton diffusion, charge separation, and charge transport, and each step is directly influenced by the nanoscale morphologies of the photoactive layers.[33,34] The interface between the donor and the acceptor materials must be sufficiently large to permit efficient exciton dissociation and interpenetrating percolation pathways are required for efficient charge transport.[4] To increase the efficiency of the photon absorption step, thick photoactive layers can potentially enhance photocurrent generation.[1,28−32] Thick photoactive layers are also easier to fabricate because their thickness may be controlled much more precisely than in thinner layers.[32] Although thick photoactive layers are advantageous for light absorption and manufacturing, they tend to decrease the device performance by the limited carrier mobility in the conjugated polymers and the increasing losses due to charge recombination.[28−32] Therefore, securing

Received: January 8, 2014
Accepted: March 26, 2014
Published: March 26, 2014

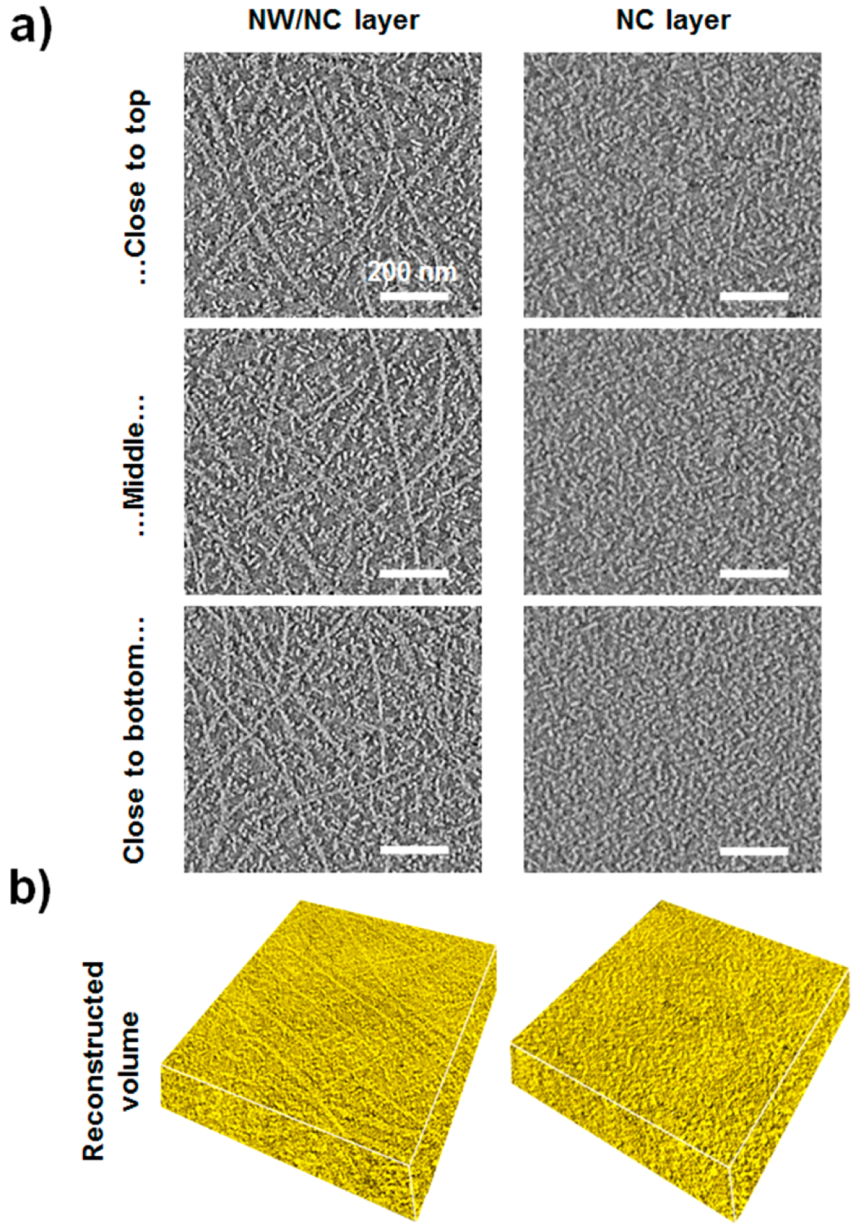

Figure 1. (a) Cross-sectional images obtained by electron tomography from the bottom to the top along the horizontal (X,Y) plane for a NW/NC blend layer and a NC blend layer. (b) Reconstructed volumes of the corresponding layers with dimensions of 900 × 900 × 200 nm.

interpenetrating percolation pathways for the charge carriers is crucially required to reduce carrier losses through recombination.

The use of self-organized polythiophene nanowires (NWs) with high crystalline ordering enables formation of interpenetrating percolation pathways for charge carrier transport, resulting in increasing the hole mobility (μ_h) to a value comparable to the electron mobility (μ_e).[7,24,25] Consequently, thick photoactive layers can be prepared by using percolated NWs without significant carrier recombination losses. Even though many efforts have been devoted to optimize the performances of device prepared with a thick active layer,[28−32] increasing the active layer thickness has received only limited attention to date. Moreover, the multidirectional percolations of polythiophene NWs and their influence on the photocurrent generation have not yet been clearly explored. The horizontal nanoscale morphologies of NWs and their interpenetrating percolations for charge carriers have been visualized.[6,12,19−28] However, the vertical percolation pathways of NWs, which are directly related to the transport of charge carriers in a real device, have not been thoroughly evaluated.

We investigated the performances of two types of photoactive layers, each with a different thickness. One layer contained high crystalline poly(3-hexylthiophene) (P3HT) NWs and small nanocrystals (NCs), yielding percolation pathways for charge carriers and the other layer contained only small NCs, bearing low percolation probability. The former was prepared with a marginal solvent and the latter was prepared with a good solvent. The three-dimensional (3D) morphologies of the active layers were analyzed by transmission electron microtomography (TEMT). The percolation probabilities of charge carriers were estimated with the sliced images along the vertical axis obtained from the 3D morphologies. The crystallinities of the layers were also investigated using grazing incident X-ray diffraction (GIXD). The influence of the P3HT crystalline structures and the photoactive layer thickness on the

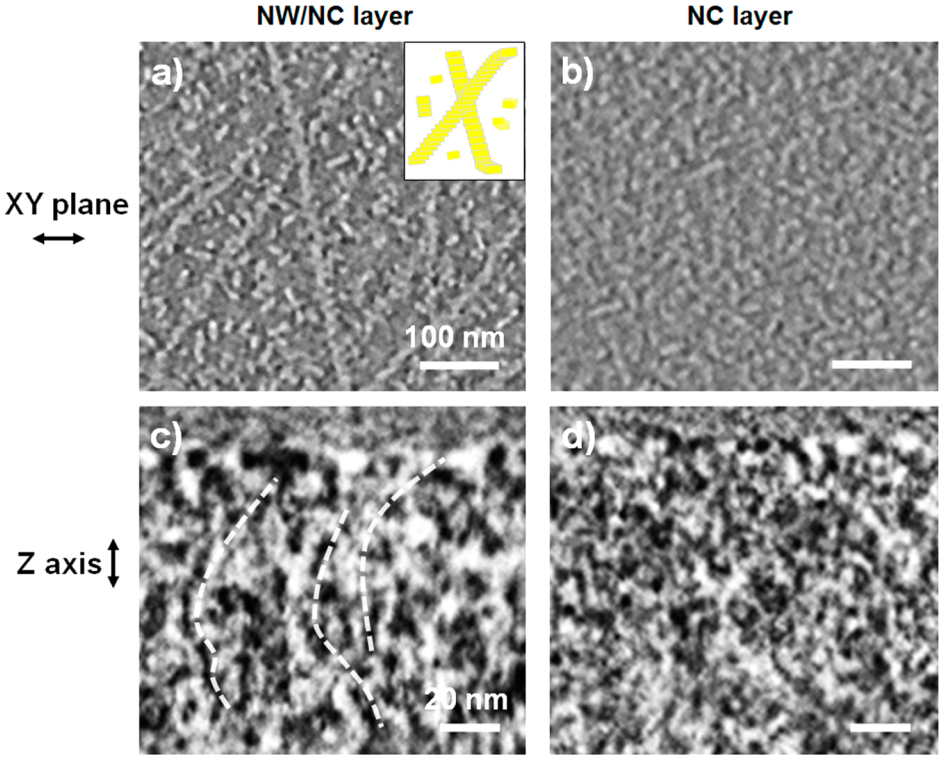

Figure 2. Magnified cross-sectional images obtained by electron tomography: (a,b) along the horizontal (X,Y) plane and (c,d) along the vertical (Z) axis for the blend layers containing P3HT NWs (a,c) and P3HT NCs (b,d). The P3HT NWs consisted of ordered small P3HT NCs, as shown in the inset.

photocurrent generation was investigated. The thickness of the photoactive layer was found to promote photon absorption, although it limited the transport of charge carriers, thereby decreasing the PCE. To circumvent this trade-off, we tested several methods of controlling the active layer morphology in an effort to produce a thick photoactive layer with highly developed pathways for charge transport. P3HT NWs were found to facilitate charge transport, thereby yielding an η_{IQE} that did not vary with the photoactive layer thickness. Finally, we demonstrated that the incorporation of P3HT NWs into a P3HT:indene-C_{60} bisadduct (ICBA) photoactive layer enhanced the performance of an OPV device, yielding a PCE of 5.42%. The photoactive layer thickness could be increased to 600 nm, yielding a slightly lower but still acceptable PCE of 3.75%.

2. EXPERIMENTAL SECTION

2.1. Materials. P3HT (4002-E), [6,6]-phenyl-C_{61}-butyric acid methyl ester (PCBM), and ICBA were purchased from Rieke Metals Inc., Nano-C Inc., and Lumtec Corp., respectively. The P3HT:PCBM (1:1, wt:wt) blend solution was prepared in a mixed solvent comprising chlorobenzene (CB) and cyclohexanone (CHN) for the fabrication of the P3HT NWs. Other solutions were prepared using CB only.

2.2. Device Fabrication and Electrical Characterization. The ITO substrates were cleaned and ozone-treated for 20 min. PEDOT:PSS (Baytron P TP AI 4083, Bayer AG) was spin-coated to a thickness of 30−35 nm and then baked at 120 °C. The photoactive layer was deposited by spin-casting the prepared blend solution onto a PEDOT:PSS-coated ITO substrate, then annealed for 10 min. The thickness of the active layers was tuned over the range 100−1000 nm by varying the concentration of the blend solutions over the range 15−25 mg mL^{-1}. The blend solutions were spin-coated at 700−3000 rpm. Ca/Al metal electrodes were deposited by thermal evaporation under high vacuum conditions (1×10^{-6} mbar). The electron and hole mobilities were measured by fabricating hole-only and electron-only devices using PEDOT:PSS/Pd and Al/Al as the anodes and cathodes, respectively. The $J-V$ characteristics were measured under AM 1.5G solar illumination at an intensity of 100 mW cm^{-2} using a source measurement unit (Keithley 4200). Light was generated using a 1 kW solar simulator (Oriel), and the light intensity was calibrated with respect to a reference silicon solar cell (PVM 132) guaranteed by the National Renewable Energy Laboratory (NREL). The IPCE was evaluated using a photomodulation spectroscopy setup (Merlin, Oriel) with monochromatic light from a xenon lamp.

2.3. Optical and Morphological Characterizations. The absolute absorption spectra for the devices were obtained by measuring the reflectance spectra using a UV−vis spectrophotometer (CARY-5000, Varian) with an integrating sphere. The GIXD patterns of the P3HT:PCBM blend films were measured at the 3C, 5A, and 9A beamlines at the Pohang Accelerator Laboratory (PAL), Korea (wavelength of approximately 1.17 Å). Film thicknesses were determined using a surface profiler (Alpha-Step 500, Tencor) and were corroborated by scanning electron microscopy (SEM) (S-4800, Hitachi). The 3D morphologies were determined using a transmission electron microscopy (TEM) instrument (JEM-2200FS, JEOL). A series of 131 two-dimensional (2D) images were obtained at tilt angles that ranged from +65° to −65° in 1° increments. The 3D images were obtained using reconstruction methods implemented in software developed previously.[35]

3. RESULTS AND DISCUSSION

3.1. Analysis of the Cross-Sectional Images and the Relative Crystallinities. The influence of the P3HT crystalline morphologies on the photocurrent generation was investigated by fabricating two different types of photoactive layers: NW/NC and NC-only active layers. The NW/NC photoactive layers containing P3HT NWs and small crystals were prepared via solubility-induced crystallization from a

mixture containing a good solvent, CB, and a marginal solvent, CHN.[25,36−38] The films were subsequently thermally annealed at the optimal temperature of 100 °C. The NC-only photoactive layers, which contained only small crystals, were prepared from the good solvent, CB, and were thermally annealed at 150 °C.

The TEMT was used to analyze the multidirectional percolations of P3HT NWs and their influence on the transport of charge carriers. The 3D structures of the specimens were reconstructed from a series of 2D projections obtained at various tilting angles with respect to the electron beam (Figure 1).[12,39,40] Image slices along the horizontal (X,Y) plane and the vertical (Z) axis were obtained from a 3D reconstruction model of the layer (Figures 1 and 2). The model revealed the organization of the layer from the bottom to the top (Figure 1). In these images, the P3HT crystals appeared to be uniformly dispersed throughout the photoactive layers as bright structures due to the electron density differences between the P3HT and PCBM component. The presence of an interpenetrating network of P3HT NWs among the coexisting small NCs was identified in the NW/NC photoactive layer (Figure 2a). The NC photoactive layer was found to consist only of small P3HT NCs (Figure 2b). All photoactive layers, regardless of the layer thickness, were characterized by the homogeneous intermixing of P3HT NWs and small NCs with the continuous amorphous P3HT and PCBM matrix. The intergrain structure of P3HT NWs was also visualized by using TEMT. The P3HT NWs were formed from self-organized small P3HT NCs, as schematically shown in the inset in Figure 2a.[41] These structures provided the intergrain connectivity in the crystallites, improving charge transport.[42] The images collected along the vertical (Z) axis, revealed intergrain percolation pathways along which the charge carriers could move throughout the vertical direction of the NW/NC photoactive layer (Figure 2c). These pathways were less extensive in the NC photoactive layer (Figure 2d). Very few connected carrier pathways were observed in the NC photoactive layer. The P3HT NWs were as long as several micrometers in length along the horizontal plane (see Figure S1 in the Supporting Information), which might not be favorable for the charge transport to the electrodes. However, the NW percolations also existed with other directions including the vertical axis, which improved overall carrier transport to the electrodes in the OSCs (Figure 2c). The percolated fractions of P3HT in the binarized vertical images of the active layers were further evaluated as the percolation probabilities of the hole carriers (Figure 7).

The crystallinity and molecular orientations of the blend films were investigated by comparing the 2D-GIXD patterns acquired from the NW/NC layer (Figure 3a) and the NC layer (Figure 3b). Quantitative estimates of the relative P3HT crystallinity were obtained by comparing the circularly averaged intensity of the 2D-GIXD patterns, as shown in Figure 3c.[43] The integrated intensity of the (100) peak of the NW/NC layer was 2.6 times the corresponding value in the NC layer, suggesting that the crystallinity of the NW/NC layer was higher than in the NC layer. The P3HT molecular chains self-organized to form lamellar crystallites that were predominantly oriented along the (100) axis ($q \approx 0.38$ Å^{-1}).[44,45] The 2D-GIXD analysis revealed that the NW/NC layer assumed an edge-on orientation in which the molecular backbones of the polymers were oriented parallel to the substrate and the side chains were oriented perpendicular to the substrate. By

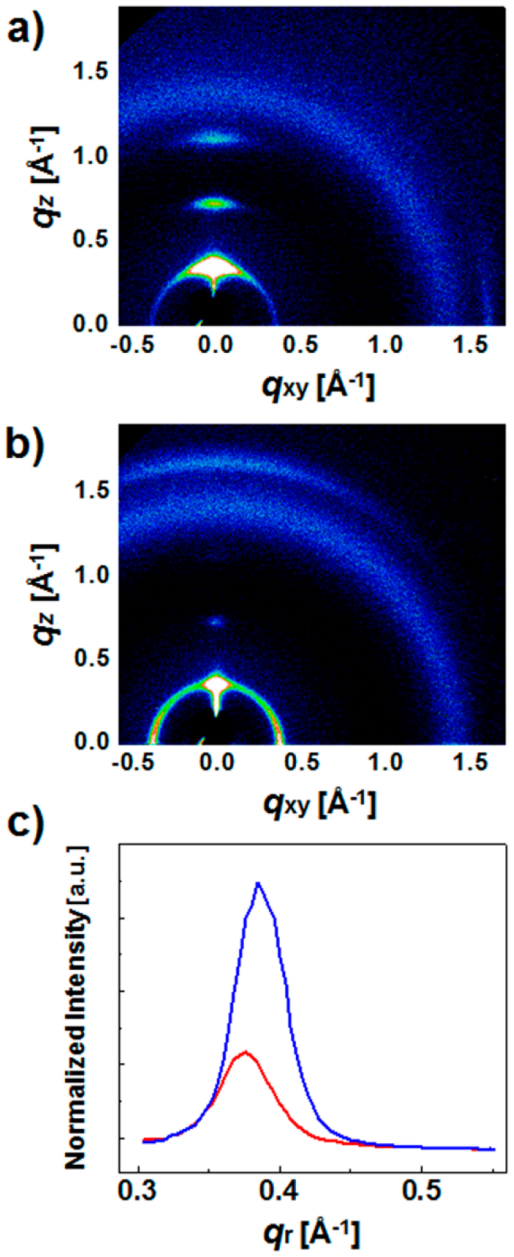

Figure 3. 2D-GIXD patterns from the P3HT:PCBM blend films containing (a) a P3HT NW/NC layer and (b) a P3HT NC layer. (c) Circularly averaged intensities from the blend films prepared from a P3HT NW/NC layer (blue) and from a P3HT NC layer (red).

contrast, the NC layer displayed mixed orientations of the crystals having edge-on or face-on polymer backbone orientations. The percolation pathways with high crystalline P3HT NWs in the NW/NC photoactive layers were expected to enhance the transport of charge carriers in solar devices prepared from these layers.

3.2. Photovoltaic Performances and Photocurrent Generation. Solar cells were fabricated using the NW/NC and NC photoactive layers, and their current density−voltage (J−V) curves were compared for various photoactive layer thickness values. As the photoactive layer thickness increased, the photovoltaic performances of the devices containing NW/NC photoactive layers improved (Figure 4a). By contrast, the performances of devices prepared with NC photoactive layers degraded (Figure 4b). The variations in the photovoltaic

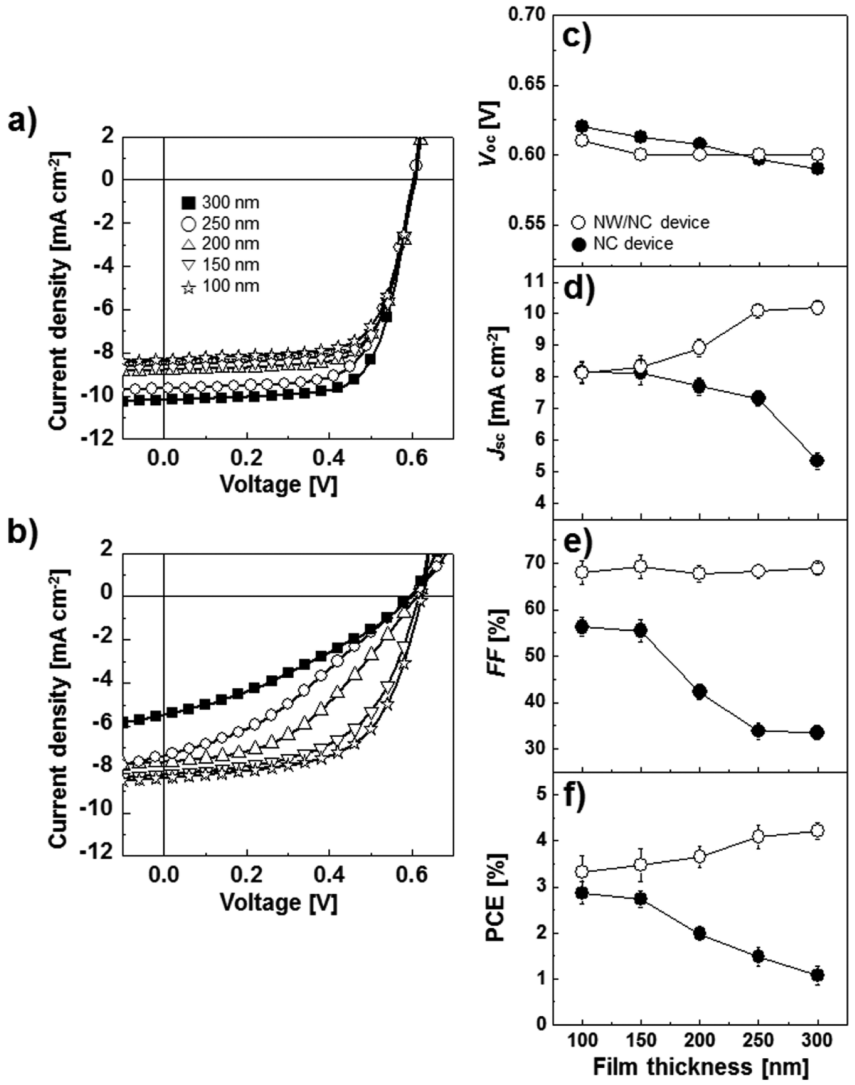

Figure 4. Current density−voltage (J−V) curves of the devices prepared with various active layer thicknesses, measured under illumination at 100 mW cm^{-2} (simulated AM 1.5G): (a) P3HT NW/NC layers and (b) P3HT NC layers. The photoactive layer thickness affected the various photovoltaic parameters of the devices: (c) V_{oc}, (d) J_{sc}, (e) FF, and (f) PCE.

Table 1. Summary of the Photovoltaic Parameters and Mobilities in Devices Prepared with P3HT:PCBM NW/NC and NC Photoactive Layers with Various Active Layer Thicknesses

	photovoltaic parameters						carrier mobilities		
thickness [nm]	V_{oc} [V]	J_{sc} [mA cm^{-2}]	FF [%]	PCE [%]	R_s [Ω cm^2]	R_{sh} [Ω cm^2]	μ_h [cm^2 V^{-1} s^{-1}]	μ_e [cm^2 V^{-1} s^{-1}]	μ_e/μ_h
for NW/NC devices									
100	0.61	8.13	68.0	3.33	1.57	1401.8	1.47×10^{-3}	1.47×10^{-3}	1.01
150	0.60	8.32	69.3	3.48	1.69	1525.9	1.55×10^{-3}	1.47×10^{-3}	0.95
200	0.60	8.92	67.7	3.66	1.79	1522.9	1.43×10^{-3}	1.39×10^{-3}	0.97
250	0.60	10.1	68.3	4.09	1.71	1464.4	1.57×10^{-3}	1.50×10^{-3}	0.96
300	0.60	10.2	68.9	4.21	1.69	1368.9	1.48×10^{-3}	1.52×10^{-3}	1.03
for NC devices									
100	0.62	8.16	56.3	2.87	1.77	950.4	9.85×10^{-5}	4.51×10^{-4}	4.58
150	0.61	8.13	55.5	2.74	1.89	704.2	1.01×10^{-4}	4.97×10^{-4}	4.92
200	0.61	7.70	42.3	1.98	1.94	698.4	1.24×10^{-4}	5.27×10^{-4}	4.24
250	0.60	7.33	33.8	1.49	2.48	220.3	9.65×10^{-5}	5.17×10^{-4}	5.36
300	0.59	5.34	33.5	1.08	5.16	243.8	9.15×10^{-5}	5.20×10^{-4}	5.68

parameters as a function of the active layer thickness were evaluated from the J−V curves and the dark J−V curves (see Figure S2 in the Supporting Information), and are shown in Figure 4c−f and Table 1. The overall PCE of the NW/NC photoactive layer devices improved significantly, from 3.33 to 4.21%, as the film thickness increased from 100 to 300 nm (Figure 4f). The performance improvement resulted mainly from an increase in the short-circuit current density (J_{sc})

dx.doi.org/10.1021/am501358k | ACS Appl. Mater. Interfaces 2014, 6, 5640−5650

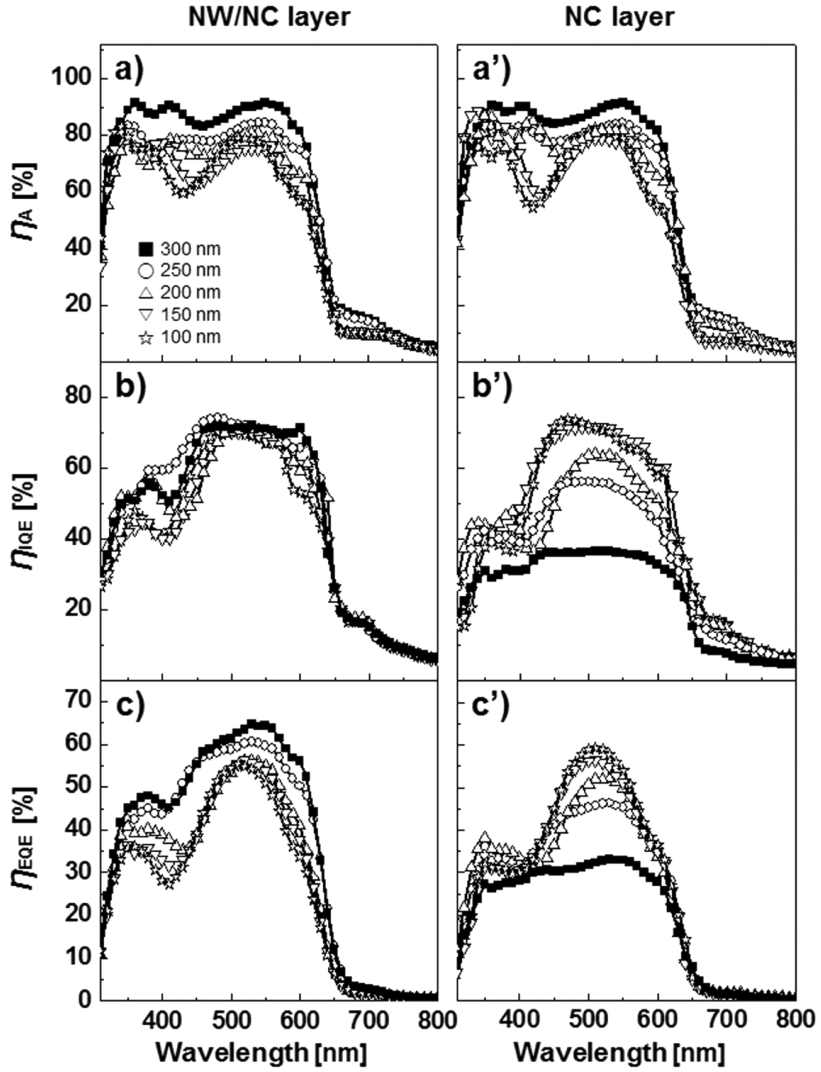

Figure 5. (a,a′) Absorption efficiencies (η_A), (b,b′) internal quantum efficiencies (η_{IQE}), and (c,c′) external quantum efficiencies (η_{EQE}) of the solar devices prepared with active layers having various thicknesses. Parameters were measured from the NW/NC blend films (a,b,c) and the NC blend films (a′,b′,c′).

because the open-circuit voltage (V_{oc}) and fill factor (FF) did not vary significantly with the photoactive layer thickness (Figure 4c–f). The high FF resulted from a low series resistance (R_s) and a high shunt resistance (R_{sh}) at all film thicknesses (Table 1). By contrast, the PCE of the NC photoactive layer devices decreased from 2.87 to 1.08% as the photoactive layer thickness increased because J_{sc}, FF, and V_{oc} all decreased as the film thickness increased from 100 to 300 nm. J_{sc} decreased from 8.16 to 5.34 mA cm^{-2}, FF decreased from 56.3 to 33.5%, and V_{oc} decreased from 0.62 to 0.59 V (Figure 4c–f). J_{sc} of the devices containing thin NC photoactive layers (100–150 nm thick) was comparable to the value of the devices containing NW/NC photoactive layers with the same thicknesses. However, J_{sc} decreased as the NC photoactive layer thickness increased. Therefore, the thick NW/NC photoactive layers were applicable to OPV devices but the thick NC photoactive layers could not be prepared for that use.

The external quantum efficiency (η_{EQE}) was calculated as the product of the efficiencies of four sequential processes: photon absorption to create an exciton (η_A), exciton diffusion to the donor–acceptor interface (η_{ED}), exciton dissociation through charge transfer (η_{CT}), and the collection of free charge carriers at the electrodes as a result of charge transport (η_{CC}).[33,34] The device performances were analyzed as functions of the crystalline morphology and photoactive layer thickness by evaluating η_A, η_{IQE}, and η_{EQE} (Figure 5):[46−50]

$$\eta_{EQE} = \eta_A \eta_{IQE} = \eta_A \eta_{ED} \eta_{CT} \eta_{CC} \quad (1)$$

The number of photons absorbed by the photoactive layer (η_A) was estimated by recording the reflectance spectra of the devices (R_d) and the electrodes (R_e) using eq. 2 (see Figure S3 in the Supporting Information):[48−50]

$$\eta_A = 100(1 - R_d/R_e) \quad (2)$$

To summarize, η_A was estimated from the measured values of R_d and R_e, η_{EQE} was measured directly, and η_{IQE} was calculated using eq. 1 (Figure 5). The number of absorbed photons increased with the film thickness for both the NW/NC (Figure 5a) and the NC (Figure 5a′) photoactive layers, and the photon absorption efficiency was not significantly affected by the P3HT crystalline ordering. The absorption efficiency of the NW/NC photoactive layer was indistinguishable from that of the NC photoactive layer for a given thickness, with a value of 91.5% for 300 nm thick layers. η_{EQE} increased significantly with the NW/

NC photoactive layer thickness (Figure 5c), in agreement with the increase in J_{sc}. η_{EQE}, on the other hand, decreased as the NC photoactive layer thickness increased, despite an increase in the number of absorbed photons (Figure 5c′). The excitons generated in the NW/NC photoactive layers appeared to be efficiently converted to a photocurrent. This conclusion was supported by the stability in η_{IQE} over the range of photoactive layer thicknesses tested (Figure 5b). By contrast, η_{IQE} decreased as the NC photoactive layer thickness increased (Figure 5b′), suggesting that the thick NC photoactive layers did not efficiently convert the photons to a photocurrent due to the relatively short crystal percolation pathways.

η_{IQE} is affected by the efficiencies of exciton dissociation and charge transport, as described by eq. 1; the use of P3HT NWs might affect not only the percolation pathways but also the interface area between the donor and the acceptor. The PL quenching efficiency of the 300 nm thick NW/NC blend film in comparison to its homo film was 94.8 ± 0.2%, which was similar to the efficiency of the NC blend film with the same thickness, 94.5 ± 0.2%; thus, exciton dissociation in the NW/NC blend film might not be much different from those in the NC blend film (see Figure S4 in the Supporting Information), assuming that the interface area between P3HT and PCBM might not be decreased significantly with the use of P3HT NWs.[51] Therefore, the variances in η_{IQE} with respect to the crystalline morphology were mainly caused by the transport of charge carriers, which was thoroughly evaluated in the following.

3.3. Charge Carrier Mobilities and Charge Transport Properties. Space-charge-limited-current (SCLC) measurements were used to evaluate the charge carrier mobilities over a range of photoactive layer thicknesses.[7,52] The dark current density values (J_D) for the hole-only and electron-only devices were multiplied by the cube of the film thickness (L) to account for variations in the blend film thickness. The J_D values are shown as functions of the applied bias, corrected for the built-in potential (see Figure S5 in the Supporting Information). The hole and electron mobilities of the devices were extracted from the J_D values of the hole-only devices and the electron-only devices, respectively (Figure 6). In the trap-free region over the trap-filled limit, the SCLC behavior could be characterized according to the Mott−Gurney square law:

$$J = (9/8)\varepsilon_0\varepsilon_r\mu(V^2/L^3) \quad (3)$$

where $\varepsilon_0\varepsilon_r$ is the permittivity of the polymer of the medium and μ is the charge carrier mobility. The hole mobilities in the NW/NC photoactive layer devices were as high as 1.57×10^{-3} cm^2 V^{-1} s^{-1}, which is 15 times higher than that observed in the NC photoactive layer devices (Table 1 and Figure 6). The electron mobilities of the NW/NC photoactive layer devices were as high as 1.52×10^{-3} cm^2 V^{-1} s^{-1} due to the formation of PCBM aggregates. This mobility is almost 3 times the value (5.27×10^{-4} cm^2 V^{-1} s^{-1}) of an NC photoactive layer device (Table 1 and Figure 6). The hole and electron mobilities of the NW/NC photoactive layers were higher than the values of the NC photoactive layers at all layer thicknesses, and the ratio of the electron mobility to the hole mobility reached unity. These results suggested that the carrier transport was balanced by a high FF. The interpenetrating P3HT NWs provided pathways for the hole carriers and induced PCBM aggregation, thereby facilitating charge transport.[24,25] These effects could not occur in the NC photoactive layers; charge transport was hampered due to the limited percolation pathways.

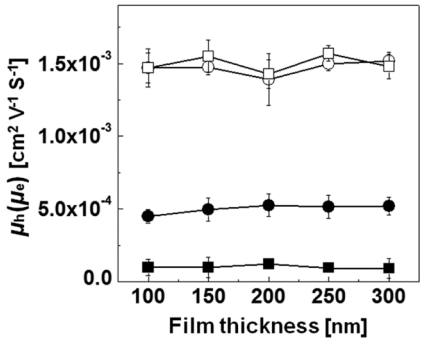

Figure 6. Hole (□) and electron mobilities (○) in the NW/NC devices were compared with the hole (■) and electron mobilities (●) in the NC devices, for various photoactive layer thicknesses.

The charge transport properties were explored by measuring the J_{sc} values in the NW/NC and NC devices prepared with various photoactive layer thicknesses as a function of the illumination intensity (P_{light}) (Figure 7a,b).[7] In general, the value of J_{sc} in a solar device followed the power-law dependence with respect to P_{light} (i.e., $J_{sc} \propto P_{light}^{S}$).[7] Over the photoactive layer thickness range of 100−300 nm, the exponential factor (S) was found to be 0.984, on average, for the NW/NC devices (Figure 7c). J_{sc} was nearly linearly dependent on the incident light. Therefore, bimolecular recombination of separated charges and space-limited charges may be greatly reduced in the NW/NC devices. The S factors did not differ significantly in the NC devices, up to a photoactive layer thickness of 150 nm (Figure 7c); however, the S factor was reduced to 0.924 in the 300 nm thick NC active layer devices, suggesting significant losses due to bimolecular recombination in the corresponding devices. The presence of these losses was further supported by the observation of limited percolation pathways and low carrier mobilities (Figure 6). The vertical percolation probabilities of the hole carriers, which affected the charge transport properties, were defined as the percolated fractions of P3HT in the binarized vertical images of the active layers (see Figure S6 in the Supporting Information).[40] Several thresholds were applied to the binarization of the images and dozens of vertical images were used to evaluate the hole percolation probabilities. The NW/NC devices displayed a hole percolation probability of 98.4 ± 0.5%, much greater than the value of 91.6 ± 1.3% observed for the NC devices (Figure 7d). The binarized vertical images from all active layer thicknesses were nearly indistinguishable for both the NW/NC and NC layers (data not shown here), suggesting that the percolation probability did not vary with the film thickness. P3HT NWs in the NW/NC layers were advantageous for forming vertical percolation paths that facilitated charge transport and reduced bimolecular recombination, yielding an η_{IQE} that was stable with the photoactive layer thickness; however, in the NC layers, charge transport was hampered due to the limited paths between relatively isolated domains (Figures 2 and 7e).

3.4. Photovoltaic Performances of the P3HT:ICBA Devices with Thick Active Layers. The mixed solvent approach to NW preparation is a simple process and is applicable to other semiconducting materials. We applied the preparation of P3HT NWs to ICBA, in which the indene units push the lowest unoccupied molecular orbital (LUMO) level close to the vacuum level, thereby increasing V_{oc} (Figures 8 and S7 in the Supporting Information).[53−57] The PCE of a device

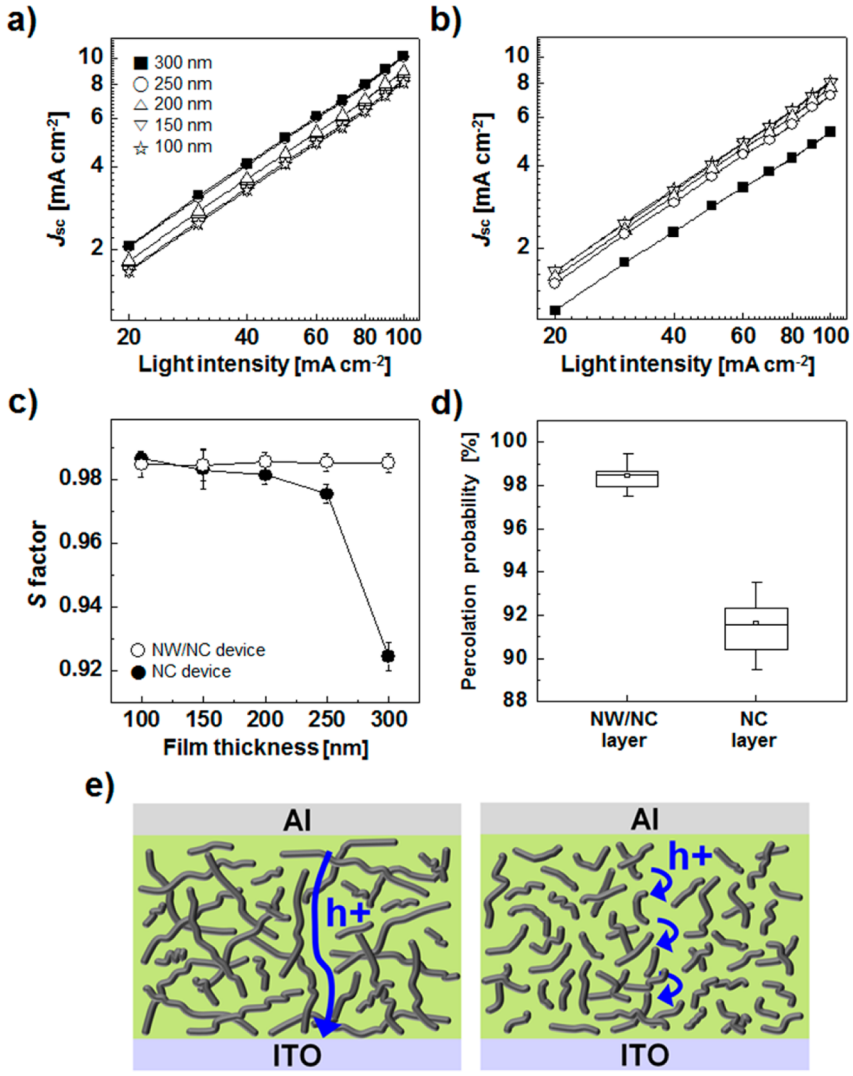

Figure 7. J_{sc} values as a function of the light intensity for (a) the NW/NC devices and (b) the NC devices. (c) *S* factors as a function of the photoactive layer thickness for the NW/NC and NC devices. (d) Estimated percolation probabilities in the NW/NC layer and in the NC layer. (e) Schematic illustrations of the vertical pathways in the NW/NC layer (left) and in the NC layer (right).

prepared with ICBA increased and the FF reached values as high as 72.4%. In the P3HT:ICBA devices prepared with NWs, the PCE was found to be 5.42%, with V_{oc} of 0.86 V, J_{sc} of 8.82 mA cm^{-2}, and FF of 71.4% for a photoactive layer thickness of 250 nm (Figure 8a and Table S1 of the Supporting Information). Thick photoactive layers yielded comparable PCEs of 4.41% (for a thickness of 400 nm) and 3.75% (for a thickness of 600 nm, Figure 8b and Table S1 of the Supporting Information) using the device structure shown in Figure 8c. The device efficiencies remained relatively constant up to a photoactive layer thickness of 600 nm, yielding a PCE that was 69.2% of the maximum photovoltaic efficiency because the J_{sc} values did not decrease significantly for layers with a higher thickness.

Thick photoactive layers are generally advantageous for their light absorption properties and their ease of processability. In this paper, we have demonstrated that the presence of an interpenetrating P3HT NW network in a photoactive layer facilitates charge transport so that the absorbed photons are converted to current without significant recombination losses. The use of thick photoactive layers containing P3HT NWs is readily applicable to OPV devices.

4. CONCLUSIONS

We compared the charge transport properties of photoactive layers prepared to contain interpenetrating NWs with the corresponding properties of layers containing only small NCs, for various active layer thicknesses. We confirmed that increasing the thickness of the photoactive layer enhanced light absorption. Further, the presence of a P3HT NW network formed interpenetrating percolation paths for efficient charge transport with low bimolecular recombination loss. Therefore, the absorbed photons were efficiently converted into an electrical photocurrent and η_{IQE} was relatively stable with the photoactive layer thickness. The use of P3HT NWs improved the performances of photovoltaic devices, yielding PCE values as high as 5.42%. A photoactive layer thickness of 600 nm yielded a PCE (3.75%) that was 70% of the maximum efficiency. We also showed that a photoactive layer containing only small P3HT NCs did not efficiently convert absorbed photons into a photocurrent. The failure of this device arose from the absence of crystalline charge transport pathways. We demonstrated that photovoltaic behavior depends critically on (1) the use of a thick photoactive layer to enhance photon

dx.doi.org/10.1021/am501358k | ACS Appl. Mater. Interfaces 2014, 6, 5640−5650

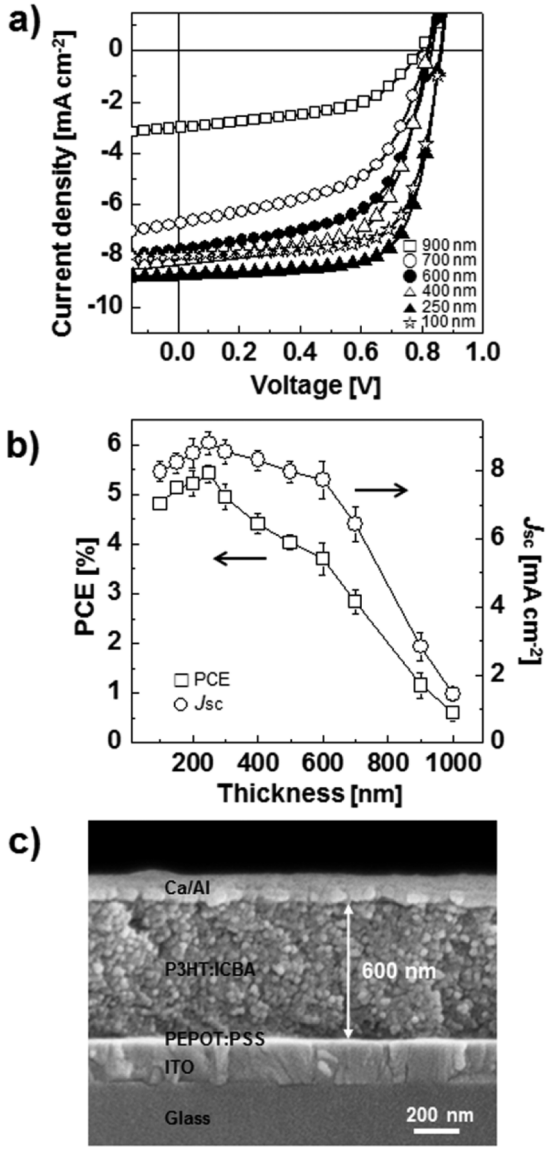

Figure 8. (a) Current density–voltage (J–V) curves and (b) PCE and J_{sc} values of the P3HT:ICBA devices containing P3HT NWs with various photoactive layer thicknesses. (c) Cross-sectional SEM image of a P3HT:ICBA device containing P3HT NWs with a photoactive layer thickness of 600 nm.

absorption and on (2) the inner structure of the photoactive layer, which can enhance photocurrent production.

■ ASSOCIATED CONTENT

Supporting Information

Further details on TEM images of P3HT nanowires, photoluminescence of the photoactive layers, dark J–V curves and reflectance spectra of the investigated solar cells, dark J–V curves of the hole and electron only devices, binarized images of the photoactive layers along the vertical axis, and J–V curves of the P3HT:ICBA devices. This material is available free of charge via the Internet at http://pubs.acs.org.

■ AUTHOR INFORMATION

Corresponding Author

*K. Cho. E-mail: kwcho@postech.ac.kr.

Notes

The authors declare no competing financial interest.

■ ACKNOWLEDGMENTS

This work was supported by a grant (Code No. 2011-0031628) from the Center for Advanced Soft Electronics under the Global Frontier Research Program of the Ministry of Science, ICT & Future Planning, Korea. The authors thank the Pohang Accelerator Laboratory for providing the synchrotron radiation sources at the 3C, 5A, and 9A beamlines used in this study.

■ REFERENCES

(1) Coakley, K. M.; McGehee, M. D. Conjugated Polymer Photovoltaic Cells. *Chem. Mater.* **2004**, *16*, 4533–4542.
(2) Thompson, B. C.; Frechet, J. M. J. Polymer-Fullerene Composite Solar Cells. *Angew. Chem., Int. Ed.* **2008**, *47*, 58–77.
(3) Yu, G.; Gao, J.; Hummelen, J. C.; Wudl, F.; Heeger, A. J. Polymer Photovoltaic Cells: Enhanced Efficiencies via a Network of Internal Donor-Acceptor Heterojunctions. *Science* **1995**, *270*, 1789–1791.
(4) Brabec, C. J.; Heeney, M.; McCulloch, I.; Nelson, J. Influence of Blend Microstructure on Bulk Heterojunction Organic Photovoltaic Performance. *Chem. Soc. Rev.* **2011**, *40*, 1185–1199.
(5) Yip, H.-L.; Jen, A. K.-Y. Recent Advances in Solution-Processed Interfacial Materials for Efficient and Stable Polymer Solar Cells. *Energy Environ. Sci.* **2012**, *5*, 5994–6011.
(6) Yang, X.; Loos, J.; Veenstra, S. C.; Verhees, W. J. H.; Wienk, M. M.; Kroon, J. M.; Michels, M. A. J.; Janssen, R. A. J. Nanoscale Morphology of High-Performance Polymer Solar Cells. *Nano Lett.* **2005**, *5*, 579–583.
(7) Mihailetchi, V. D.; Xie, H.; de Boer, B.; Koster, L. J. A.; Blom, P. W. M. Charge Transport and Photocurrent Generation in Poly (3-Hexylthiophene):Methanofullerene Bulk-Heterojunction Solar Cells. *Adv. Funct. Mater.* **2006**, *16*, 699–708.
(8) Ma, W.; Yang, C.; Gong, X.; Lee, K.; Heeger, A. J. Thermally Stable, Efficient Polymer Solar Cells with Nanoscale Control of the Interpenetrating Network Morphology. *Adv. Funct. Mater.* **2005**, *15*, 1617–1622.
(9) Lee, J. H.; Park, J. H.; Kim, J. S.; Lee, D. Y.; Cho, K. High Efficiency Polymer Solar Cells with Wet Deposited Plasmonic Gold Nanodots. *Org. Electron.* **2009**, *10*, 416–420.
(10) Li, G.; Shrotriya, V.; Huang, J.; Yao, Y.; Moriarty, T.; Emery, K.; Yang, Y. High-Efficiency Solution Processable Polymer Photovoltaic Cells by Self-Organization of Polymer Blends. *Nat. Mater.* **2005**, *4*, 864–868.
(11) Park, J. H.; Kim, J. S.; Lee, J. H.; Lee, W. H.; Cho, K. Effect of Annealing Solvent Solubility on the Performance of Poly(3-Hexylthiophene)/Methanofullerene Solar Cells. *J. Phys. Chem. C* **2009**, *113*, 17579–17584.
(12) van Bavel, S. S.; Sourty, E.; de With, G.; Loos, J. Three-Dimensional Nanoscale Organization of Bulk Heterojunction Polymer Solar Cells. *Nano Lett.* **2009**, *9*, 507–513.
(13) Jo, S. B.; Lee, J. H.; Sim, M.; Kim, M.; Park, J. H.; Choi, Y. S.; Kim, Y.; Ihn, S.-G.; Cho, K. High Performance Organic Photovoltaic Cells Using Polymer-Hybridized ZnO Nanocrystals as a Cathode Interlayer. *Adv. Energy Mater.* **2011**, *1*, 690–698.
(14) Lee, J. K.; Ma, W. L.; Brabec, C. J.; Yuen, J.; Moon, J. S.; Kim, J. Y.; Lee, K.; Bazan, G. C.; Heeger, A. J. Processing Additives for Improved Efficiency from Bulk Heterojunction Solar Cells. *J. Am. Chem. Soc.* **2008**, *130*, 3619–3623.
(15) Peet, J.; Kim, J. Y.; Coates, N. E.; Ma, W. L.; Moses, D.; Heeger, A. J.; Bazan, G. C. Efficiency Enhancement in Low-Bandgap Polymer Solar Cells by Processing with Alkane Dithiols. *Nat. Mater.* **2007**, *6*, 497–500.
(16) Gu, Y.; Wang, C.; Russell, T. P. Multi-Length-Scale Morphologies in PCPDTBT/PCBM Bulk-Heterojunction Solar Cells. *Adv. Energy Mater.* **2012**, *2*, 683–690.
(17) Vohra, V.; Higashimine, K.; Murakami, T.; Murata, H. Addition of Regiorandom Poly(3-Hexylthiophene) to Solution Processed

Poly(3-Hexylthiophene):[6,6]-Phenyl-C_{61}-Butyric Acid Methyl Ester Graded Bilayers to Tune the Vertical Concentration Gradient. *Appl. Phys. Lett.* **2012**, *101*, 173301.
(18) Liao, H.-C.; Tsao, C.-S.; Shao, Y.-T.; Chang, S.-Y.; Huang, Y.-C.; Chuang, C.-M.; Lin, T.- H.; Chen, C.-Y.; Su, C.-J.; Jeng, U.-S.; Chen, Y.-F.; Su, W.-F. Bi-Hierarchical Nanostructures of Donor-Acceptor Copolymer and Fullerene for High Efficient Bulk Heterojunction Solar Cells. *Energy Environ. Sci.* **2013**, *6*, 1938−1948.
(19) Berson, S.; De Bettignies, R.; Bailly, S.; Guillerez, S. Poly (3-Hexylthiophene) Fibers for Photovoltaic Applications. *Adv. Funct. Mater.* **2007**, *17*, 1377−1384.
(20) Moule, A. J.; Meerholz, K. Controlling Morphology in Polymer-Fullerene Mixtures. *Adv. Mater.* **2008**, *20*, 240−245.
(21) Xin, H.; Reid, O. G.; Ren, G.; Kim, F. S.; Ginger, D. S.; Jenekhe, S. A. Polymer Nanowire/Fullerene Bulk Heterojunction Solar Cells: How Nanostructure Determines Photovoltaic Properties. *ACS Nano* **2010**, *4*, 1861−1872.
(22) Xin, H.; Kim, F. S.; Jenekhe, S. A. Highly Efficient Solar Cells Based on Poly(3-Butylthiophene) Nanowires. *J. Am. Chem. Soc.* **2008**, *130*, 5424−5425.
(23) Zhao, Y.; Shao, S.; Xie, Z.; Geng, Y.; Wang, L. Effect of Poly (3-Hexylthiophene) Nanofibrils on Charge Separation and Transport in Polymer Bulk Heterojunction Photovoltaic Cells. *J. Phys. Chem. C* **2009**, *113*, 17235−17239.
(24) Kim, J. S.; Lee, J. H.; Park, J. H.; Shim, C.; Sim, M.; Cho, K. High-Efficiency Organic Solar Cells Based on Preformed Poly(3-Hexylthiophene) Nanowires. *Adv. Funct. Mater.* **2011**, *21*, 480−486.
(25) Kim, J.-H.; Park, J. H.; Lee, J. H.; Kim, J. S.; Sim, M.; Shim, C.; Cho, K. Bulk Heterojunction Solar Cells Based on Preformed Polythiophene Nanowires via Solubility-Induced Crystallization. *J. Mater. Chem.* **2010**, *20*, 7398−7405.
(26) Tsoi, W. C.; Nicholson, P. G.; Kim, J. S.; Roy, D.; Burnett, T. L.; Murphy, C. E.; Nelson, J.; Bradley, D. D. C.; Kim, J.-S.; Castro, F. A. Surface and Subsurface Morphology of Operating Nanowire:Fullerene Solar Cells Revealed by Photoconductive-AFM. *Energy Environ. Sci.* **2011**, *4*, 3646−3651.
(27) Williams, E. L.; Gorelik, S.; Phang, I.; Bosman, M.; Vijila, C.; Subramanian, G. S.; Sonar, P.; Hobley, J.; Singh, S. P.; Matsuzaki, H.; Furube, A.; Katoh, R. Nanoscale Phase Domain Structure and Associated Device Performance of Organic Solar Cells Based on a Diketopyrrolopyrrole Polymer. *RSC Adv.* **2013**, *3*, 20113−20124.
(28) Moule, A. J.; Meerholz, K. Intensity-Dependent Photocurrent Generation at the Anode in Bulk-Heterojunction Solar Cells. *Appl. Phys. B: Lasers Opt.* **2008**, *92*, 209−218.
(29) Lenes, M.; Koster, L. J. A.; Mihailetchi, V. D.; Blom, P. W. M. Thickness Dependence of the Efficiency of Polymer:Fullerene Bulk Heterojunction Solar Cells. *Appl. Phys. Lett.* **2006**, *88*, 243502.
(30) Sievers, D. W.; Shrotriya, V.; Yang, Y. Modeling Optical Effects and Thickness Dependent Current in Polymer Bulk-Heterojunction Solar Cells. *J. Appl. Phys.* **2006**, *100*, 114509.
(31) Price, S. C.; Stuart, A. C.; Yang, L.; Zhou, H.; You, W. Fluorine Substituted Conjugated Polymer of Medium Band Gap Yields 7% Efficiency in Polymer-Fullerene Solar Cells. *J. Am. Chem. Soc.* **2011**, *133*, 4625−4631.
(32) Li, W.; Hendriks, K. H.; Roelofs, W. S. C.; Kim, Y.; Wienk, M. M.; Janssen, R. A. J. Efficient Small Bandgap Polymer Solar Cells with High Fill Factors for 300 nm Thick Films. *Adv. Mater.* **2013**, *25*, 3182−3186.
(33) Moliton, A.; Nunzi, J.-M. How to Model the Behaviour of Organic Photovoltaic Cells. *Polym. Int.* **2006**, *55*, 583−600.
(34) Peumans, P.; Yakimov, A.; Forrest, S. R. Small Molecular Weight Organic Thin-Film Photodetectors and Solar Cells. *J. Appl. Phys.* **2003**, *93*, 3693−3723.
(35) Jinnai, H.; Spontak, R. J. Transmission Electron Microtomography in Polymer Research. *Polymer* **2009**, *50*, 1067−1087.
(36) Lim, J. A.; Kim, J.-H.; Qiu, L.; Lee, W. H.; Lee, H. S.; Kwak, D.; Cho, K. Inkjet-Printed Single-Droplet Organic Transistors Based on Semiconductor Nanowires Embedded in Insulating Polymers. *Adv. Funct. Mater.* **2010**, *20*, 3292−3297.
(37) Zhang, L.; Colella, N. S.; Liu, F.; Trahan, S.; Baral, J. K.; Winter, H. H.; Mannsfeld, S. C. B.; Briseno, A. L. Synthesis, Electronic Structure, Molecular Packing/Morphology Evolution, and Carrier Mobilities of Pure Oligo-/Poly(Alkylthiophenes). *J. Am. Chem. Soc.* **2013**, *135*, 844−854.
(38) Park, Y. D.; Lee, H. S.; Choi, Y. J.; Kwak, D.; Cho, J. H.; Cho, K. Solubility-Induced Ordered Polythiophene Precursors for High-Performance Organic Thin-Film Transistors. *Adv. Funct. Mater.* **2009**, *19*, 1200−1206.
(39) Yang, X.; Loos, J. Toward High-Performance Polymer Solar Cells: The Importance of Morphology Control. *Macromolecules* **2007**, *40*, 1353−1362.
(40) Li, S.-S.; Chang, C.-P.; Lin, C.-C.; Lin, Y.-Y.; Chang, C.-H.; Yang, J.-R.; Chu, M.-W.; Chen, C.-W. Interplay of Three-Dimensional Morphologies and Photocarrier Dynamics of Polymer/TiO_2 Bulk Heterojunction Solar Cells. *J. Am. Chem. Soc.* **2011**, *133*, 11614−11620.
(41) Lee, E.; Hammer, B.; Kim, J.-K.; Page, Z.; Emrick, T.; Hayward, R. C. Hierarchical Helical Assembly of Conjugated Poly(3-Hexylthiophene)-Block-Poly(3-Triethylene Glycol Thiophene) Diblock Copolymers. *J. Am. Chem. Soc.* **2011**, *133*, 10390−10393.
(42) Rivnay, J.; Mannsfeld, S. C. B.; Miller, C. E.; Salleo, A.; Toney, M. F. Quantitative Determination of Organic Semiconductor Microstructure from the Molecular to Device Scale. *Chem. Rev.* **2012**, *112*, 5488−5519.
(43) Bottiger, A. P. L.; Jorgensen, M.; Menzel, A.; Krebs, F. C.; Andreasen, J. W. High-Throughput Roll-to-Roll X-Ray Characterization of Polymer Solar Cell Active Layers. *J. Mater. Chem.* **2012**, *22*, 22501−22509.
(44) Kim, D. H.; Park, Y. D.; Jang, Y.; Yang, H.; Kim, Y. H.; Han, J. I.; Moon, D. G.; Park, S.; Chang, T.; Chang, C.; Joo, M.; Ryu, C. Y.; Cho, K. Enhancement of Field-Effect Mobility Due to Surface-Mediated Molecular Ordering in Regioregular Polythiophene Thin Film Transistors. *Adv. Funct. Mater.* **2005**, *15*, 77−82.
(45) Oh, J. Y.; Shin, M.; Lee, T. I.; Jang, W. S.; Min, Y.; Myoung, J.-M.; Baik, H. K.; Jeong, U. Self-Seeded Growth of Poly(3-Hexylthiophene) (P3HT) Nanofibrils by a Cycle of Cooling and Heating in Solutions. *Macromolecules* **2012**, *45*, 7504−7513.
(46) Slooff, L. H.; Veenstra, S. C.; Kroon, J. M.; Moet, D. J. D.; Sweelssen, J.; Koetse, M. M. Determining the Internal Quantum Efficiency of Highly Efficient Polymer Solar Cells through Optical Modeling. *Appl. Phys. Lett.* **2007**, *90*, 143506.
(47) Burkhard, G. F.; Hoke, E. T.; Scully, S. R.; McGehee, M. D. Incomplete Exciton Harvesting from Fullerenes in Bulk Heterojunction Solar Cells. *Nano Lett.* **2009**, *9*, 4037−4041.
(48) Jo, J.; Na, S.-I.; Kim, S.-S.; Lee, T.-W.; Chung, Y.; Kang, S.-J.; Vak, D.; Kim, D.-Y. Three-Dimensional Bulk Heterojunction Morphology for Achieving High Internal Quantum Efficiency in Polymer Solar Cells. *Adv. Funct. Mater.* **2009**, *19*, 2398−2406.
(49) Dennler, G.; Forberich, K.; Scharber, M. C.; Brabec, C. J.; Tomis, I.; Hingerl, K.; Fromherz, T. Angle Dependence of External and Internal Quantum Efficiencies in Bulk-Heterojunction Organic Solar Cells. *J. Appl. Phys.* **2007**, *102*, 054516.
(50) Park, S. H.; Roy, A.; Beaupre, S.; Cho, S.; Coates, N.; Moon, J. S.; Moses, D.; Leclerc, M.; Lee, K.; Heeger, A. J. Bulk Heterojunction Solar Cells with Internal Quantum Efficiency Approaching 100%. *Nat. Photonics* **2009**, *3*, 297−303.
(51) He, X.; Gao, F.; Tu, G.; Hasko, D. G.; Huttner, S.; Greenham, N. C.; Steiner, U.; Friend, R. H.; Huck, W. T. S. Formation of Well-Ordered Heterojunctions in Polymer:PCBM Photovoltaic Devices. *Adv. Funct. Mater.* **2011**, *21*, 139−146.
(52) Goodman, A. M.; Rose, A. Double Extraction of Uniformly Generated Electron-Hole Pairs from Insulators with Noninjecting Contacts. *J. Appl. Phys.* **1971**, *42*, 2823−2830.
(53) He, Y.; Chen, H.-Y.; Hou, J.; Li, Y. Indene-C_{60} Bisadduct: A New Acceptor for High-Performance Polymer Solar Cells. *J. Am. Chem. Soc.* **2010**, *132*, 1377−1382.
(54) Liao, S.-H.; Li, Y.-L.; Jen, T.-H.; Cheng, Y.-S.; Chen, S.-A. Multiple Functionalities of Polyfluorene Grafted with Metal Ion-

Intercalated Crown Ether as an Electron Transport Layer for Bulk-Heterojunction Polymer Solar Cells: Optical Interference, Hole Blocking, Interfacial Dipole, and Electron Conduction. *J. Am. Chem. Soc.* **2012**, *134*, 14271−14274.

(55) Nardes, A. M.; Ferguson, A. J.; Whitaker, J. B.; Larson, B. W.; Larsen, R. E.; Maturova, K.; Graf, P. A.; Boltalina, O. V.; Strauss, S. H.; Kopidakis, N. Beyond PCBM: Understanding the Photovoltaic Performance of Blends of Indene-C_{60} Multiadducts with Poly(3-Hexylthiophene). *Adv. Funct. Mater.* **2012**, *22*, 4115−4127.

(56) Kang, T. E.; Cho, H.-H.; Cho, C.-H.; Kim, K.-H.; Kang, H.; Lee, M.; Lee, S.; Kim, B.; Im, C.; Kim, B. J. Photoinduced Charge Transfer in Donor-Acceptor (DA) Copolymer: Fullerene Bis-adduct Polymer Solar Cells. *ACS Appl. Mater. Interfaces* **2013**, *5*, 861−868.

(57) Thummalakunta, L. N. S. A.; Yong, C. H.; Ananthanarayanan, K.; Luther, J. P3HT Based Solution-Processed Pseudo Bi-Layer Organic Solar Cell with Enhanced Performance. *Org. Electron.* **2012**, *13*, 2008−2016.